GOLD Observations of Longitudinal Variations in the Nighttime Equatorial Ionization Anomaly (EIA) Crests' Latitudes

R. W. Eastes[1], D. K. Karan[1], C. Martinis[2], R. E. Daniell[3], Q. Gan[1], A. G. Burns[4], and W. E. McClintock[1]

[1]Laboratory for Atmospheric and Space Physics, University of Colorado, Boulder, CO, USA,
[2]Center for Space Physics, Boston University, Boston, MA, USA,
[3]Ionospheric Physics, Stoughton, MA, USA,
[4]High Altitude Observatory, National Center for Atmospheric Research, Boulder, CO, USA,

Corresponding author: Richard Eastes (richard.eastes@lasp.colorado.edu)

Key Points:

- The average nighttime EIA crests' latitudes observed by GOLD during 2020 equinoxes and December solstice have a longitudinal dependence
- Crests' latitude dependence on longitude changes near 47°W geographic, where the magnetic and geographic equators cross
- Crests' latitudes over 75°W-10°E geographic longitude during equinoxes and winter solstice depend on the subsolar point magnetic latitude

Abstract

Each day the GOLD (Global-scale Observations of the Limb and Disk) imager observes the Equatorial Ionization Anomaly (EIA) near sunset from ~10° E to ~80° W geographic longitude. Most images cover ~45° of longitude (~3 hours), and most longitudes are observed multiple times. Monthly averages of EIA crests' latitude (EIA lats) versus longitude during March, September and December 2020 have been analyzed. The EIA lats reflect the combined influence of winds, solar radiation, and fields (electric and magnetic) in the equatorial region. Winter solstice differs significantly from the equinoxes, which are similar, but there are notable similarities between all three. The similarities in the EIA lats during the seasons examined indicates that the magnetic equator to subsolar point separation influences them in all three seasons and that it has a more distinct, possibly more significant, influence than winds on the average latitudes.

Plain Language Summary

Each day the GOLD (Global-scale Observations of the Limb and Disk) imager observes the nighttime Equatorial Ionization Anomaly (EIA) near sunset as the terminator progresses westward from Africa to across South America. Most images cover ~45° of longitude (~3 hours of local time), and most longitudes are observed multiple times. In 2020 seasonal averages of the crests' latitude versus longitude during the equinoxes (March and September) and winter solstice (December) show significant, important similarities. The observed latitude versus longitude dependence in all three show a dependence on the distance between the magnetic equator and the subsolar point. Greater knowledge of the seasonal-longitudinal dependence of the EIA crests' latitudes contributes significantly to understanding the crests' response to fields (electric and magnetic) and winds in the equatorial region.

1 Introduction

Longitudinal differences in the EIA are a source of information about spatial differences in the processes that influence their creation and decay. Changes in their radiance have often been linked to differences in the equatorial electrojet (EEJ) strength which are attributable to longitudinal differences in solar tidal forcing (England et al., 2006; Fang et al., 2009; Jin et al., 2008; Lühr et al., 2008; Pedatella et al., 2012; Lühr & Manoj, 2013; Venkatesh et al., 2015; Yamazaki and Maute, 2016; Zhou et al., 2016; Mo and Zhang, 2020). Variations in the optical dayglow radiances at the northern crest's latitudes over Indian longitudes show a similar relationship with the EEJ strength (Karan et al., 2016). The small scale (3^o-7^o) longitudinal differences in the dayglow radiances have been attributed to variations of the equatorial electric fields (Karan et al., 2017). Differences in the EEJ and and tides might also alter the latitudes. While there have been multiple studies of the EIA radiances, the longitudinal dependence of the EIA crests' latitudes (EIA lats), where the radiances peak, is less studied. Observing such effects is complicated by longitudinal variation in both the location of the magnetic equator and the magnetic declination at the equator as well as neutral winds which are additional influences on the EIA.

Significant short term variability is seen in the EIA lats. Recently, Rodríguez-Zuluaga, et al. (2021) found that the EIA lats observed by GOLD sometimes exhibit a mesoscale structure (a few thousand km scale size), indicating that they may be influenced by waves from the lower atmosphere. Other periodic, longitudinal variations in the EIA crests' brightnesses are also seen (e.g., Eastes et al., 2019, Fig 3; Gan et al 2020, Fig. 2), as are occasional decreases in their

separation (e.g., Basu et al., 2009). Such decreases have sometimes been sufficient to reduce the two crests typically observed to a single crest located near the magnetic equator (e.g., Aa et al. 2022).

The EIA around the South Atlantic Anomaly (SAA), where largest low-latitude deviations in Earth's magnetic field occur, is one of the most interesting longitude regions. The magnetic equator is north of the geographic equator near Africa and south of it over South America, Unfortunately, concurrent observations of the EIA across the SAA region have been insufficient for a comprehensive study. Both ground and space based observations have limitations - there are few ground based observations over Africa and radiation in the South Atlantic Anomaly (SAA) can interfere with space-based observations by low Earth orbiting satellites (e.g., Kil et al., 2006). These same longitudes, in and near the SAA, are observed during GOLD's nighttime disk imaging. Each night GOLD, whose orbit places it safely above radiation in the SAA, routinely images the EIA crests throughout this region. These images provide an opportunity to study the EIA and, possibly, to better understand it at all longitudes.

Every evening the GOLD mission observes the same region of the EIA near sunset with sufficient signal-to-noise to locate the EIA crests over South America, the Atlantic Ocean, and West Africa. This paper presents our analysis of EIA lats versus longitude during both equinoxes and December solstice in 2020, a solar minimum year with relatively quiet geomagnetic conditions. Monthly averages are used to simplify the identification of systematic, global-scale dependences. Such averages suppress the effects of short term variability in the EEJ and the winds. Any remaining, distinct patterns should be indicative of underlying processes that influence the EIA. The results indicate that the EIA lats have an often neglected dependence on the latitude of the subsolar point.

2 Data

The observations used in the analysis are nighttime, partial disk scans by the GOLD imager, which is hosted on the SES 14 satellite in geostationary orbit at 47.5° W. The instrument and its observations have been described by McClintock et al. (2020a, b) and Eastes et al. (2017, 2020). Each of the two, independent channels contains a scan mirror and interchangeable slits, enabling each channel to observe either the northern or southern hemisphere.

During 2020 GOLD conducted nightside imaging observations (partial disk scans, NI1 mode) daily, beginning at 1700 satellite local time (SLT) (2010 UT) with a 30-min cadence, using only one channel (designated as channel B), alternating between the northern and southern hemispheres. At 2000 SLT (2310 UT), when both channels were used for nightside scans, both hemispheres were imaged simultaneously at a 15-min cadence. This imaging continued until 2130 SLT (0040 UT) when observations were suspended to avoid accidentally observing the Sun. Each night 24 images (each covering half the latitudes) were obtained. The medium-resolution slit used during the partial-disk scans provides ~0.3 nm spectral resolution and a spatial resolution of ~93 km (96 km × 80 km) at the sub-satellite location (0° geographic latitude, 47.5° W longitude). Observations were made at a constant angular resolution.

Most individual scans cover ~45° in longitude, ~3 hours in local time, just east of the sunset terminator. Scans shift westward throughout the evening, observing the low latitudes from ~8° E to ~80° W longitude. Each scan images EIA locations from ~1 hour after sunset to later local times. The observation sequence is described in detail by Karan, et al. (2020). At night the EIA typically appears as bands of enhanced OI 135.6 nm emission, one on each side of the magnetic equator.

An example of the EIA images (from March 30, 2020) can be seen in Figure 1(a). The OI 135.6 nm emission altitude is assumed to be 300 km, a typical altitude for the F region peak, when geolocating the pixels. An example of the EIA lats obtained from the nightly sequence of images is shown in Figure 1(b) where each data point represents a peak in a crest's brightness (the method is described in Section 3). The geographic longitude corresponding to the magnetic longitude (used during the analysis) is also shown in this figure.

The OI 135.6 nm emission from the EIA is produced by recombination of atomic oxygen ions and electrons in the Earth's ionosphere. In the F region oxygen ions are the dominant ion species. Since the emission rate varies approximately as the square of the electron density, as $n_e \times n_{O+}$, the observed radiance is dominated by emissions from near the peak in electron density and is indicative of the peak plasma density, N_{max}.

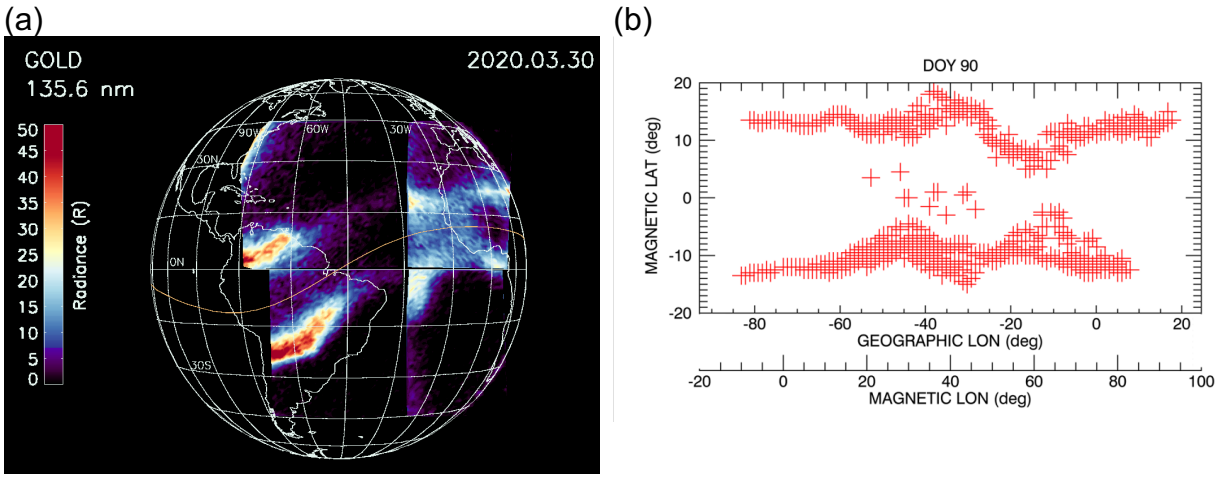

Figure 1. (1a) Composite image constructed from portions of four nightside (NI1) images taken on March 30, 2020. The geographic latitude variation of the EIA crests with geographic longitude seen in these images can be clearly seen in the crests' peak latitudes, as shown in (1b) after mapping into magnetic coordinates. (1b) Both crests' latitudes identified in nightside images from March 30, 2020 (DOY 90) at latitudes within 21° of the magnetic equator are included in the analysis. At most longitudes there are multiple images of the crests, hence multiple latitudes are shown in 1b.

This paper examines the nightside, NI1 observations during March, September and December 2020. The first two months are near equinox and the latter is near winter solstice in the northern hemisphere, periods when bright emissions are observed from the EIA. Bright emissions allow a more accurate and consistent determination of the EIA lats; brightnesses during June solstice were too low to obtain good statistics or sufficient longitudinal coverage. In June crest latitudes were retrieved on only 9 days and only over Africa. Geomagnetic conditions, which can be a significant influence on the EIA lats, were relatively quiet during most of these three months. A notable exception was a late September CIR storm (Sept. 22-30; Karan et al., 2021), which was excluded from the analysis. After excluding that storm, any changes associated with the remaining Dst and ap fluctuations during March, September and December (Figure 2) have little effect in monthly averages.

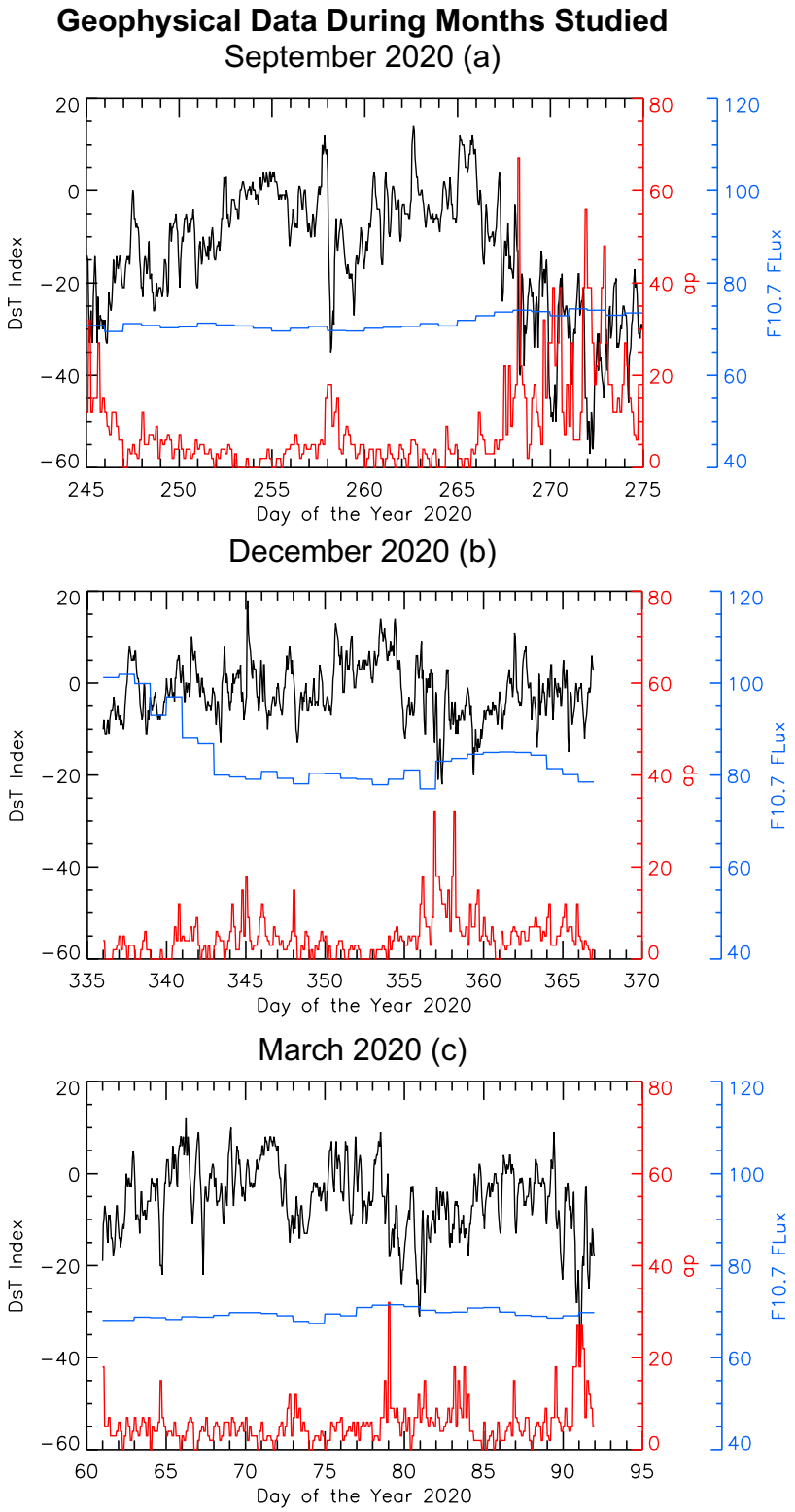

Figure 2. Geophysical data for September, December and March 2020. The Dst and ap indexes are plotted in black and red, respectively. The F10.7 index is plotted in blue. Crest latitudes during the CIR storm in late September (22-30) were excluded from the monthly average.

132

3 Analysis Method

While the GOLD data are mapped into geographic coordinates during processing, the EIA crests are more readily analyzed in their natural coordinates, magnetic. Therefore, all images are remapped using the quasi-dipole (QD) magnetic coordinates corresponding to the observed geographic coordinates (Laundal and Richmond, 2017; Thébault et al., 2021). A one day sequence of such images is shown in supplementary Figure S1. From the remapped images, the OI 135.6 nm radiance as a function of magnetic latitude (mlat) is obtained for each 1° in magnetic longitude (mlon). These radiances are smoothed over 3 points (i.e., 1.5° in mlat), and the maxima correspond to the EIA lats used in subsequent analysis. Following this procedure, EIA lats are obtained for each night. An example, from March 30, is shown in Figure 1(b).

While longitudes near the western edge of South America are measured only once each night (see the data points near 80° W in Figure 1b), most longitudes are sampled multiple times, typically 4-5 times. Consequently, multiple crest latitudes are identified at most longitudes on a given night (see Figure S1). While there is some variation in the EIA lats, due to the signal-to-noise limitations of the data, the latitudinal changes with longitude shown in Figure 1b are consistent with the images shown in Figure 1a and the other images (Figure S1) from March 30. A similar correspondence is typically seen throughout March, September and December 2020. Therefore, the observed latitude versus longitude dependence is primarily attributable to the EIA development prior to the earliest NI1 observations, which was ~1 hour after sunset. While the EIA brightness typically decreases with time due to recombination, the latitude-longitude variation appears to persist from the earliest to the latest observations. During GOLD's observations (1700-2130 SLT; 2010-0040 UTC, observations end on the following day) the observed latitudes are more indicative of the crests' development before 1700-2130 SLT.

Before further processing, the crests' latitudes in each 1° mlon bin for a day (e.g., as in Figure 1b) were filtered to remove outliers (crest latitudes likely attributable to noise). Filtering removed latitudes (a) deviating by more than half the mean value (when ≥ 3° latitudes were available in the bin), (b) attributable to known artifacts in the data, or (c) at magnetic latitudes greater than 21°, 22°, and 30° from the magnetic equator in the March, September and December observations respectively. From the EIA lats satisfying these conditions, a daily mean was calculated for each hemisphere, north and south, using 5° magnetic longitude bins. The monthly average of the crests' magnetic latitudes as a function of mlon for September is shown in Figure 3a. Magnetic latitudes of the northern and southern (absolute value) crests are plotted as red ○'s and blue ×'s, respectively. The latitudes shown have been smoothed over three, 5° longitude bins. The average latitudes of the crests (north and south) are plotted as green *'s. The error bars are representative of the ±1σ standard deviations at selected longitude bins. However, the latitudes are not completely independent, substantial correlations (>0.6 in Sept.) occur between the latitude displacements from the means for widely separated longitudes. Consequently, differences persisting across multiple longitudes can be meaningful even when they are smaller than the error bars for individual longitude bins. Persistent deviations that are of similar magnitude to the uncertainties shown but persist for numerous longitude bins are plausibly significant. Such behavior is also consistent with the influence of physical processes in the thermosphere and ionosphere having spatial scales larger than the longitudinal grid used.

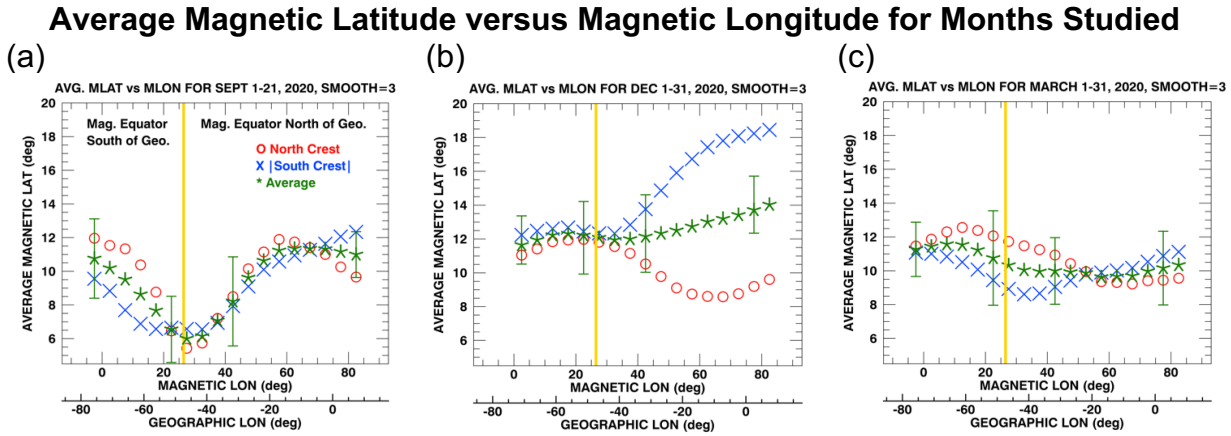

Figure 3. Monthly average of the absolute value of the magnetic latitude of the EIA crests as a function of magnetic longitude (green *) for (a) September (equinox), (b) December (solstice), and (c) March 2020 (equinox). Also shown are the latitudes of the northern crest (red ○), and absolute value of southern crest (blue ⨯). (See text for a complete explanation of the averaging process). The yellow vertical line at 26.5° mlon indicates the longitude where the magnetic and geographic equators cross. The magnetic latitude shifts are consistent with displacing both crests in the same geographic direction. The changes in separation and location near where the equators cross indicate there are significant seasonal-longitudinal differences in the EIA latitudes.

4 Results and Discussion

As shown in Figure 3a and 3c, during equinox the monthly averaged EIA lats have a minimum near 26.5° magnetic longitude (vertical, yellow line, ~50° W geographic longitude). Each of the crests, north and south, exhibits a slightly different longitude dependence. The crests in both hemispheres show similar trends during Fall and Spring equinox. Relative to the north-south averages, the southern crests in the west are at slightly lower latitudes (~2º) than the northern, and the displacements reverse at the most eastern longitudes. During December solstice even larger southward shifts, ~4º, are seen at the eastern longitudes. These shifts are consistent with a southward shift, geographically, of both crests which, at the eastern longitudes, increases the magnetic latitude of the southern crest and decreases that of the northern. These relatively consistent patterns in the monthly averages indicate that identifiable processes are probably responsible, that the shifts are not random.

As discussed in the introduction the EIA lats and their symmetry with respect to the magnetic equator depend on several influences, including the ion production and loss rates (primarily at local times prior to sunset), neutral winds, tides, electric fields (e.g., Fang et al., 2018), and magnetic field configuration. Next, these influences on the nighttime crests' latitudes are discussed.

Neutral winds, tides and electric fields: Since the effects of neutral winds, tides and the resulting electric fields are intertwined, their effect will be discussed jointly. Each is a possible source of latitudinal shifts. Shifts due to meridional winds have been reported (e.g., Khadka et al., 2018 and references therein). Both longitudinal (e.g. England et al., 2006) and seasonal (e.g. Hedin et al., 1991 or Liu et al., 2006) differences in the winds are widely recognized. These differences may introduce seasonal (equinox versus solstice) and the longitudinal (east versus west) signatures in the EIA lats. Similarly, longitudinal differences in the winds have been associated with tides.

One of the most prominent differences in the winds due to tides is associated with the landmass distribution (e.g., England et al., 2006). Since most of the eastern longitude region that GOLD observes is over the Atlantic while the western longitudes are over South America, stronger DE3 tides and associated tidal intereactions (Oberheide et al., 2011) would be expected at the western longitudes. Consequently, similar longitudinal effects would be expected at solstice and equinox, but there are significant seasonal differences. Therefore, other effects or combination of effects appear to have a larger influence on the EIA lats.

Seasonal differences in the meridional winds are associated with differences in the solar energy received, north versus south. Models and the available observations both indicate that the winds are similar for all three seasons.

Winds from HWM 14 (Drob et al., 2015) near the start of the observations, approximately one hour after sunset, are similar at all the longitudes and months that GOLD observed. For example, in September, at both 75° W (near the maximum separation) and 45° W (near the minimum) northward winds reach ~10 m/s and zonal winds ~100 m/s at latitudes near the EIA. Winds could shift the crests' latitudes northward, increasing northern and decreasing southern latitudes. Winds also alter the neutral composition slightly (Liu et al., 2009), which would slightly alter ion production and loss (discussed later) rates, but the effects are expected to be small. At the western longitudes, where the largest displacements are seen, the northward latitude shifts shown in Figure 3a for September are consistent with those from HWM 14. However, the HWM 14 winds in December are inconsistent with the observations because the crests at the eastern longitudes are shifted opposite the meridional winds. The data used in HWM 14 could be a factor. HWM 14 is expected to perform best in the American sector where it was updated from a previous version to include ground-based observations from the American sector and the South Pole. The model incorporates fewer data from the African sector where Fisher et al., (2015) reported Fabry-Perot Interferometer measurements from the Ukaimeden Observatory in Morocco (31.2° N, 7.9°W; 19.7° magnetic) from Nov 2013 to Dec 2014 that differ from the model.

However, longitudinally averaged dayside observations by the Ionospheric CONnections (ICON) mission also show northward winds, consistent with HWM 14, during all three months. ICON observed significantly (2-5 times) stronger winds at low latitudes during solstice (Figure 4). Immel et al., (2021) found, in 23-31 March 2020 ICON observations, meridional ion velocities at the equator that varied with longitude (e.g., their Figure 3) but were smaller (< 10 m/s) than the mean, equatorial neutral winds in Figure 4. The ion velocities observed in March are even less significant relative to the neutral winds in September and December. Without the strong northward winds during solstice, even larger southward displacements would be expected.

Nightside winds during the GOLD observations are probably northward also. Since the available observations are consistent HWM 14 on the dayside, it is plausible to infer nightside winds from HWM 14. Since those are also northward, significant longitudinal differences in the average neutral winds would be necessary to explain the observed latitudes. This seems unlikely for all three months. During both equinoxes the EIA crests are displaced northward over South America but southward over Africa. Similarly, during December only the eastern longitudes are significantly displaced relative to the magnetic equator. These results are consistent with dayside processes playing a key role in the post-sunset structure of the EIA crests. Furthermore, this indicates that the observed displacements probably have other or additional causes than winds alone.

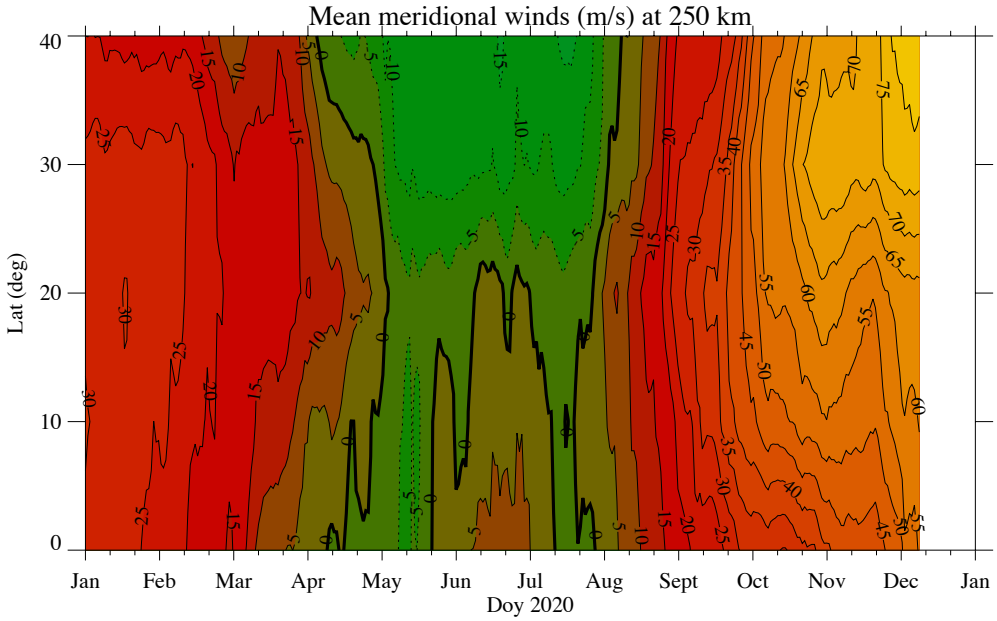

Figure 4. Mean meridional winds at 250 km observed by ICON as function of latitude and day of 2020. Tides have been removed.

Winds can also influence the vertical drifts, which have been linked to the strength of the EIA, but few studies have investigated the longitude dependence. Fejer et al. (2008) have shown that during equinox upward drifts increase from ~70° W to 0° in the evening (see their Figure 8). Therefore, their observations would not explain the longitude dependence shown in Figure 3. Kil et al. (2008) used ROCSAT-1 data to extract vertical plasma drifts near the equator and found a wave-4 pattern that was used to reproduce a similar pattern in electron density (Fang et al., 2009). Models have shown similar results (e.g., Pedatella et al., 2011). Since the wave-4 pattern is a tidal effect further discussion is presented in the next section.

Magnetic declination, PRE and PSSR: In addition to the electric fields associated with the neutral winds, there are longitudinally localized field effects in the pre-reversal enhancement (PRE) and post sunset rise (PSSR), both of which have longitudinal-seasonal variations related to the magnetic declination. These are a recognized cause of longitudinal differences in the EIA, and the largest declinations at low-latitude are over South America. GOLD nighttime observations encompass these longitudes which also have the largest offsets between Earth's magnetic and geographic latitudes. At the westernmost and easternmost longitudes, the magnetic declination δ is near zero. Near the region where magnetic and geographic equators cross, δ is ~ -20° as shown in Figure 5. Consequently, the interaction between constant winds and the Earth's magnetic field can vary substantially with longitude, and similar effects are expected during Spring and Fall equinoxes. If we denote the geographic zonal and meridional wind components as U_G and V_G, then the magnetic meridional component can be expressed as $V_M = V_G \cos(\delta) \mp U_G \sin(\delta)$ (equation 3 of Luan and Solomon, 2008). Note that, the equatorward meridional wind components are positive – i.e., southward directed in the northern hemisphere and northward in the southern hemisphere – and the upper (lower) sign applies to the northern (southern) hemisphere. Consequently, V_M and V_G can differ significantly when δ is nonzero and a strong zonal wind is present. Thus, longitudinal asymmetries in the crests can occur, depending on the local magnetic field configuration. Eastward of the equators crossing, approximately where changes in the crests' latitudes occur, V_M decreases;

273 therefore, one should expect the minimum displacements and symmetric locations if wind-
274 magnetic field effects dominante. Since the observed latitudes during some months are clearly
275 inconsistent with that expectation, that effect alone is clearly insufficient.

276 The magnetic declination angle also affects the PRE which is stronger when the sunset
277 terminator and magnetic field lines are aligned (Abdu et al., 1981; Tsunoda, 1985). These effects
278 are most prominent over eastern South America, resulting in stronger postsunset vertical ion drifts
279 during December solstice, when the sunset terminator and magnetic field lines are more aligned
280 than during June solstice, as observed in AE-E and ROCSAT-1 measurements (Fejer et al.,1995,
281 2008). Fejer et al. (2008, Figure 8) found that the seasonal, longitudinal variation of PRE during
282 December solstice had a maximum at ~45° W. That does not match the observed variations the
283 EIA lats in December (Figure 3b). During eqinox, the PRE trends higher rom 75°W to 0° longitude,
284 which does not match the observed EIA latitudinal variation (Figures 3a, 3c). Therefore,
285 longitudinal differences in PRE (alone) would not explain the observed EIA latitudes.

286 Even though the PRE is weak the PSSR of the F layer, to which PRE contributes, can be
287 strong (Tsunoda et al., 2018). The similarity between the longitudinal behavior of the EIA crests
288 latitudes in September (Figure 3a) and the magnetic declination versus longitude plot, shown in
289 Figure 5, prompted us to examine the solar terminator to magnetic field alignment. Because, when
290 the terminator and magnetic field are aligned, sunset is near simultaneous at magnetically
291 conjugate points, as discussed earlier. Since this can enhance the PSSR, producing conditions
292 favorable for ionospheric depletions and scintillation, it might also influence the EIA latitudes.
293 Figure 6 shows how the average magnetic latitude changes with the magnetic declination to solar
294 terminator (D-T) angle for March (blue), September (red), December (green), at locations west
295 (+, × or ✱) and east (◊, ★ or ○) of the minimum declination. For equinox the terminator is
296 assumed to be parallel to the latitude meridians; for December solstice the average inclination to
297 the meridians (21.2°) is assumed.

298 As seen from Figure 6, there is no apparent dependence on the declination-terminator angle
299 in March and December. If the D-T alignment alone were responsible for the observed longitudinal
300 changes in magnetic latitude, a similar dependence should occur during both equinoxes. It should
301 also be expected during December solstice because the D-T angles over Africa reach similar values
302 to those during equinox over South America. In December the D-T angle varies significantly
303 across the longitudes observed, and as discussed earlier, east of ~40° W longitude both crests are
304 offset south (magnetically) relative to the magnetic equator. Clearly the D-T alignment alone is
305 not the dominant factor in determining the EIA lats.

306 The large latitude shifts observed during December solstice probably eliminate the PSSR
307 electric fields from a primary role. During December previous analyses at solar minimum indicate
308 that the average PSSR would be weak over the longitudes with large shifts. Consequently, a ~4°
309 shift in latitude seems unlikely during the brief ~1 hour period typical for the PSSR. Also, the
310 observed latitude of the EIA at each longitude is observed from ~1 hour after sunset to later local
311 times and changes little during the evening hours. Similarly, comparisons with TEC data from
312 earlier local times appear to show a similar latitude versus longitude structure pre and post sunset
313 (e.g., Cai et al., 2020). To summarize, since latitude shifts of ~4° are observed and these shifts do
314 not show a distinct dependence on the D-T angle, additional mechanisms must be significant and
315 declination effects alone cannot explain the observed crests' latitudes.

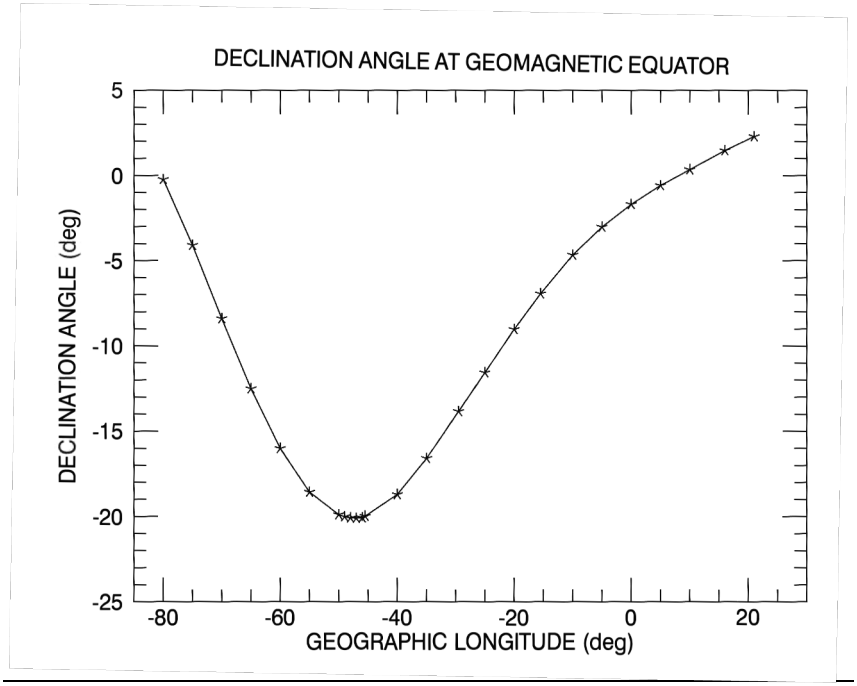

Figure 5. At equinox the angle between the solar terminator and the magnetic field is approximately the declination angle. Declination angles from https://www.ngdc.noaa.gov/geomag/calculators/magcalc.shtml.

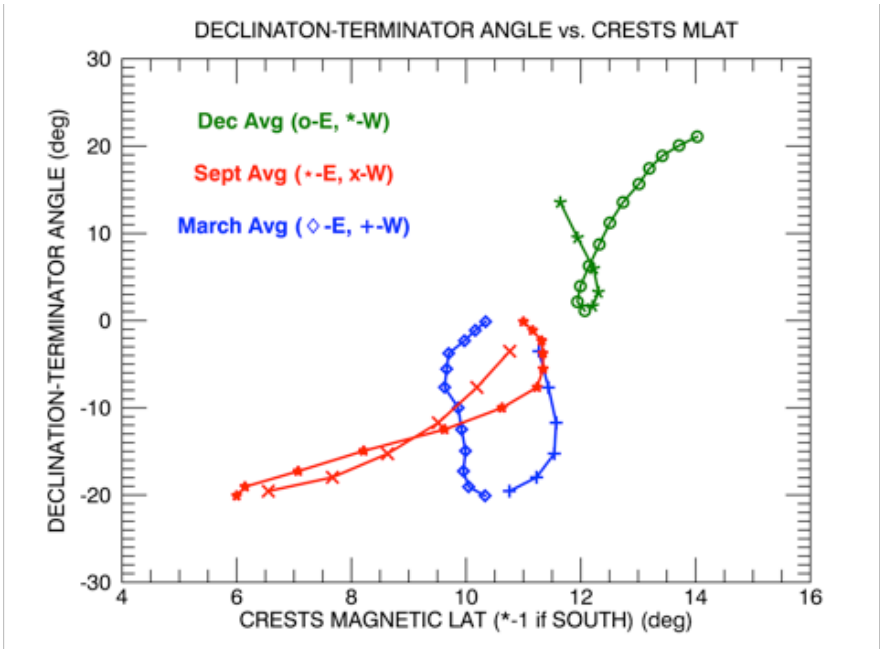

Figure 6. The dependence of the crests' average latitude on the magnetic declination to terminator (D-T) angle in December and March are similar. Both differ from September. This indicates that other factors must influence the latitudes. Averaged magnitudes of the EIA lats for March, September and December are shown in blue, red and green respectively. For each month points west (+, × or ✱) and east (◊, ★ or ○) of the minimum declination are shown.

Ionization and radiative recombination: Ion production at night is insignificant, essentially all the nighttime ionosphere is residual ionization produced during the daytime. While

the daytime production provides the initial ion densities which the other processes modify, resulting in the peak densities GOLD observes. Radiative recombination ($O^+ + e^-$) can play a more important role. It influences the peak electon densites and TEC in the nighttime ionosphere. Since winds preferentially move ions along the magnetic field, the peak altitude of ionosphere in the equatorial region also changes, increasing or decreasing as they move along the magnetic field. As the altitude increases (decreases) the volume number densities decrease (increase) which decreases (increases) the recombination rates. Consequently, asymmetries in the peak densities are likely to increase with time. Radiative recombination effects should not significantly affect the average locations shown in Figure 3 because all longitudes are observed near sunset, at similar local times. This expectation is consistent with a small set of GOLD images of the Eastern longitudes were an additional images were made at later local times. Those images were approximately 1 hour later than the first images near Africa. Changes in the EIA latitude were small even with approximately twice the time since sunset. Given the seasonal dependence of the neutral winds, etc. radiative recombination is expected to influence the observed latitudes of the EIA, but it is expected to be a small effect based on the observations. That expectation is consistent with modeling (Cai et al., 2022) for times when distinct changes in the EIA latitude are observed on an hour time scale. Furthermore, observations of such rapid changes in latitude are atypical in the GOLD data.

Subsolar point: There is an additional seasonal effect to consider beyond those associated with the winds, tides, and magnetic field geometry discussed above: the subsolar point location. During both equinoxes the subsolar point at most longitudes over South America is north of the magnetic equator and south of it over the Atlantic Ocean and Africa. During December solstice the subsolar point to magnetic equator separation reaches ~30° at longitudes over the Atlantic Ocean and Africa. Shown in Figure 7 is the average separation for each month analyzed. Average values for the two equinox months, September and March, differ slightly because days during the CIR storm in late September were omitted. Some dependence on the subsolar point is not surprising since ion production rates on the dayside have a solar zenith angle dependence and the nightside ionosphere in the EIA within a few hours of sunset (where GOLD observes) consists primarily of ions produced on the dayside.

The equinox observations exhibit a dependence on the subsolar point location at longitudes where the separation between the equators is greatest within GOLD's field-of-regard (FOR). The EIA lats in March and September, Figure 3a and 3c, show northward displacements (north crests to higher and south crests to lower magnetic latitudes) of both crests at most longitudes west of ~ -40° W. Shifts in the opposite direction are seen at the most eastern longitudes but are less prominent, although the subsolar-magnetic equator separation is similar in both the east and west.

A dependence on the subsolar point location is also consistent with the December observations (Figure 3b) and the stronger, northward winds during solstice. At the eastern longitudes the crests are displaced as much as 6° southward, but in the west displacements are negligible. If the subsolar point location were the only influence, as seen from Figure 7 one would expect similar latitude changes at the western longitudes for both seasons since subsolar-equator separations are similar.

A similar dependence on subsolar point to magnetic equator separation has been reported for dayside observations. Balan et al. (2013) found that the north-south asymmetry of TEC in the EIA at equinox during magnetically quiet conditions seemed more dependent on the displacement of the equators than on the declination angle. They examined Constellation Observing System for Meteorology Ionosphere and Climate (COSMIC) data and found weaker asymmetries at smaller

magnetic equator displacements (15° W-75° W geographic) than at larger (60° E-120° E and 60° W-120° W). As shown in their Figure 1, the displacements within GOLD's FOR have similar maximum absolute values in the Eastern (~10° W geographic) and Western (~70° W) observations, but GOLD shows more prominent displacements at the Western longitudes. Although their results indicated that the declination angle is a significant factor in the TEC asymmetry, that is not apparent in GOLD's peak density observations. As in GOLD's observations, their TEC data indicated that the displacement of the equators is a significant factor.

Likewise, a study of daytime GNSS TEC asymmetries in the 110° E geographic longitude sector during the 2000 to 2011 solar cycle by Huang et al. (2013) also found that the subsolar point location helped explain changes in the EIA. Their results indicated that the magnetic declination angle was also a factor but did not quantify the relative contribution. The observations from GOLD indicate that the subsolar point is a significant factor at night also, that its average influence may be more significant than that of neutral winds, tides or magnetic declination. Consequently, the subsolar point should be considered when examining the EIA lats (e.g., Oyedokun et al., 2020) at longitudes where the equators have significant separation.

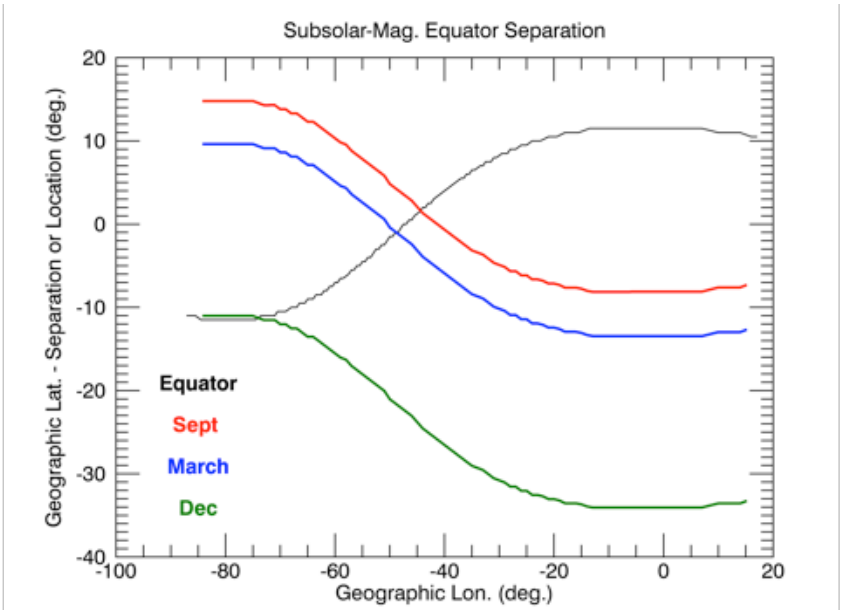

Figure 7. Each month studied has the same separation change with longitude but the mean subsolar-magnetic equator distances differ. March and September differ because some geomagnetically disturbed days during the latter were excluded. The geographic latitudes of the magnetic equator shown were used to calculate the mean separation from the subsolar point.

Since ion production rates are highest at the subsolar point a depdence on it during the daytime is expected. Some dependence at night, especially near sunset, should be expected since changes in the distribution are a result of time dependent processes that occur after the ions are produced. Depending on the rate of these processes and the time of the observations, the ionospheric densities observed at night can and should have a significant dependence on the local ion production rates on the dayside. Effects from the other processes discussed earlier (winds, tides, PSSR, PRE, etc.) will influence the electron distrution, but all begin with the electron production rates on the dayside. Electron production maximizes at the minimum solar zenith angle, corresponding to the subsolar point. GOLD's observations indicate that at solar minimum the

average nightime EIA latitude for times near sunset is not completely dependent on the processes occurring after the ions are produced.

Conclusions

Monthly averaged latitudes of the EIA crests from GOLD nightside disk (NI1) observations show statistically significant differences during geomagnetically quiet conditions. Observations from two equinox (March and September) and one solstice (December) months of 2020 were analyzed. The magnetic latitudes of the north and south crests during all three months (Figure 3) have a different dependence on longitude.

Several possible causes for the observed changes were considered. The influence of winds, tides, and magnetic fields (declination) were not consistently distinguishable over seasons and longitudes. Since data from GOLD cover the same range of EIA longitudes (~80° W to 10° E geographic) each day, the observed variations with longitude were examined for consistency with the longitudal dependence of each possible cause of latitude changes with longitude. While winds, tides and magnetic declination will contribute to the observed changes, all of them were inconsistent with the observed behavior. For example in December, the crests over Africa are displaced southward while those over South America were not displaced, although the neutral winds should be northward and similar in both regions.

One influence that does appear to be consistent with the observed latitude changes in all three months is the subsolar point to magnetic equator separation. As the distance to the magnetic equator increases at either the east or west longitudes, both the northern and southern crests exhibit shifts toward the subsolar point. For example, during December solstice both crests are shifted southward by as much as ~6° at longitudes over Africa where the subsolar point is south of the magnetic equator by as much as ~30° but are near the equator at longitudes over South America where the subsolar point is near the magnetic equator. In the data examined there is a correspondence between the latitudinal displacement of the crests and distance between the subsolar point and magnetic equator.

While some previous studies of TEC in the daytime EIA found both the subsolar point and the magnetic declination have identifiable effects, GOLD's observations of the peak densites in the nighttime EIA indicate that the subsolar point dependence is the most distinct in seasonal averages . Since previous studies spanning a complete solar cycle found similar effects in daytime TEC during solar minimum and maximum, the effects observed by GOLD during solar minimum are also expected during solar maximum. Further studies, including simulations and modeling, that consider all the influences on the location of the EIA crests will be needed to understand the effects of each in GOLD's observations.

These results suggest that GOLD's observations of the nightside EIA structure could provide a daily picture of the integrated effects of ionospheric processes, with information about the longitudinal differences in the low latitude processes from western South America to Western Africa. Since LEO satellite observations at low latitudes over South America are frequently problematic due to the South Atlantic Anomaly (SAA), GEO observations of that region provide a unique opportunity to expand our understanding of the thermosphere-ionosphere system.

Acknowledgments and Data

This research was supported by NASA contract 80GSFC18C0061to the University of Colorado.

Open Reserch

The geomagnetic indices and solar flux data are obtained from https://omniweb.gsfc.nasa.gov/. The GOLD data used in this study are available from the GOLD Science Data Center (http://gold.cs.ucf.edu/search/) and NASA's Space Physics Data Facility (https://spdf.gsfc.nasa.gov/pub/data/gold/).

References

Aa, E., Zhang, S.-R., Wang, W., Erickson, P. J., Qian, L., Eastes, R., et al. (2022). Pronounced suppression and X-pattern merging of equatorial ionization anomalies after the 2022 Tonga volcano eruption. Journal of Geophysical Research: Space Physics, 127, e2022JA030527. https://doi.org/10.1029/2022JA030527

Abdu, M. A., J. A. Bittencourt, and I. S. Batista (1981). Magnetic declination control of the equatorial F-region dynamo electric field development and spread-F, *J. Geophys. Res. Space Physics*, 86, 11,443–11,446, doi:10.1029/JA086iA13p11443

Alken, P., Thébault, E., Beggan, C.D. et al. (2021). International Geomagnetic Reference Field: the thirteenth generation. Earth Planets Space **73**, 49. doi:10.1186/s40623-020-01288-x

Balan, N., Rajesh, P.K., Sripathi, S., Tulasiram, S., Liu, J.Y., and Bailey, G.J. (2013). Modeling and observations of the north–south ionospheric asymmetry at low latitudes at long deep solar minimum; *Advances in Space Research,* **52** 375–382, doi:10.1016/j.asr.2013.04.003.

Basu, Su., Basu, S., Huba, J., Krall, J., McDonald, S. E., Makela, J. J., Miller, E. S., Ray, S., and Groves, K. (2009). Day-to-day variability of the equatorial ionization anomaly and scintillations at dusk observed by GUVI and modeling by SAMI3, *J. Geophys. Res. Space Physics*, 114, A04302, doi:10.1029/2008JA013899

Cai, X., Burns, A. G., Wang, W., Coster, A., Qian, L., Liu, J., ... & McClintock, W. E. (2020). Comparison of GOLD nighttime measurements with total electron content: Preliminary results. *J. Geophys. Res. Space Physics, 125*(9), e2019JA027767. doi:10.1029/2019JA027767

Cai, X., Qian, L., Wang, W., McInerney, J. M., Liu, H.-L., & Eastes, R. W. (2022). Hemispherically asymmetric evolution of nighttime ionospheric equatorial ionization anomaly in the American longitude sector. Journal of Geophysical Research: Space Physics, 127, e2022JA030706. doi:10.1029/2022JA030706

Drob, D. P., Emmert, J. T., Meriwether, J. W., Makela, J. J., Doornbos, E., Conde, M., et al. (2015). An update to the Horizontal Wind Model (HWM): The quiet time thermosphere, *Earth and Space Science*, *2*, 301–319, doi:10.1002/2014EA000089

Eastes, R. W., McClintock, W. E., Burns, A. G., Anderson, D. N., Andersson, L., Codrescu, M., et al. (2017). The Global-scale Observations of the Limb and Disk (GOLD) mission. *Space Sci Rev*, 212, 383, doi:10.1007/s11214-017-0392-2

Eastes, R. W., Solomon, S. C., Daniell, R. E., Anderson, D. N., Burns, A. G., England, S. L., Martinis, C. R., & McClintock, W. E. (2019). Global-scale observations of the equatorial ionization anomaly. *Geophysical Research Letters, 46, 9318-9326,* doi:10.1029/2019GL084199*h*

Eastes, R. W., McClintock, W. E., Burns, A. G., Anderson, D. N., Andersson, L., Aryal, S., et al. (2020). Initial observations by the GOLD mission. *J. Geophys. Res. Space Physics*, *125*, e2020JA027823, doi:10.1029/2020JA027823

England, S. L., Maus, S., Immel, T. J., & Mende, S. B. (2006). Longitudinal variation of the *E* region electric fields caused by atmospheric tides. *Geophysical Research Letters*, *33*, L21105, doi:10.1029/2006GL027465

Fang, T.-W., Kil, H., Millward, G., Richmond, A. D., Liu, J.-Y., & Oh, S.-J. (2009). Causal link of the wave-4 structures in plasma density and vertical plasma drift in the low-latitude ionosphere. *J. Geophys. Res. Space Physics*, *114*, A10315, doi:10.1029/2009JA014460

Fang, T.-W., Fuller-Rowell, T., Yudin, V., Matsuo, T., & Viereck, R. (2018). Quantifying the sources of ionosphereday-to-day variability. *J. Geophys. Res. Space Physics*, 123,9682–9696. doi:10.1029/2018JA025525

Fejer, B. G., E. R. de Paula, R. A. Heelis, and W. B. Hanson (1995). Global equatorial ionospheric vertical plasma drifts measured by the AE-E satellite, *J. Geophys. Res. Space Physics*, 100(A4), 5769–5776, doi:10.1029/94JA03240

Fejer, B. G., J. W. Jensen, and S.-Y. Su (2008). Quiet time equatorial F region vertical plasma drift model derived from ROCSAT-1 observations, *J. Geophys. Res. Space Physics*, 113, A05304, doi:10.1029/2007JA012801

Fisher, D. J., J. J. Makela, J. W. Meriwether, R. A. Buriti, Z. Benkhaldoun, M. Kaab, and A. Lagheryeb (2015). Climatolo- gies of nighttime thermospheric winds and temperatures from Fabry-Perot interferometer mea- surements: From solar minimum to solar maximum, *J. Geophys. Res. Space Physics*, *120*, 6679–6693, doi:10.1002/2015JA021170

Forbes, J. M., Maute, A., Zhang, X., & Hagan, M. E. (2018). Oscillation of the ionosphere at planetary-wave periods. *J. Geophys. Res. Space Physics*, 123, 7634–7649 doi:10.1029/2018JA025720

Gan, Q., W. Wang, J. Yue, H. Liu, L. C. Chang, S. Zhang, A. Burns, and J. Du (2016). Numerical simulation of the 6 day wave effects on the ionosphere: Dynamo modulation, *J. Geophys. Res. Space Physics*, 121, 10,103–10,116, doi:10.1002/2016JA022907

Gan, Q., Eastes, R. W., Burns, A. G., Wang, W., Qian, L., Solomon, S. C., et al. (2020). New observations of large‐scale waves coupling with the ionosphere made by the GOLD Mission: Quasi‐16‐day wave signatures in the F‐region OI 135.6‐nm nightglow during sudden stratospheric warmings. *J. Geophys. Res. Space Physics*, 125, e2020JA027880, doi:10.1029/2020JA027880

Hedin, A. E., Biondi, M. A., Burnside, R. G., Hernandez, G., Johnson, R. M., Killeen, T. L., ... & Virdi, T. S. (1991). Revised global model of thermosphere winds using satellite and ground-based observations. *Journal of Geophysical Research: Space Physics*, *96*(A5), 7657-7688.

Huang, L., Huang, J., Wang, J., Jiang, Y., Deng, B., Zhao, K., & Lin, G. (2013). Analysis of the north–south asymmetry of the equatorial ionization anomaly around 110 E longitude. *Journal of Atmospheric and Solar-Terrestrial Physics*, *102*, 354-361. doi:10.1016/j.jastp.2013.06.010

Jin, H., Miyoshi, Y., Fujiwara, H., & Shinagawa, H. (2008). Electrodynamics of the formation of ionospheric wave number 4 longitudinal structure. *J. Geophys. Res. Space Physics*, *113*, A09307.doi:10.1029/2008JA013301

Immel, T. J., Harding, B. J., Heelis, R. A., Maute, A., Forbes, J. M., England, S. L., ... & Makela, J. J. (2021). Regulation of ionospheric plasma velocities by thermospheric winds. *Nature geoscience*, *14*(12). 893-898., doi:10.1038/s41561-021-00848-4

Karan, D. K., D. Pallamraju, K. A. Phadke, T. Vijayalakshmi, T. K. Pant, and S. Mukherjee (2016). Electrodynamic influence on the diurnal behavior of neutral daytime airglow emissions. *Ann. Geophys*., 34, 1019-1030, doi:10.5194/angeo-34-1019-2016

Karan, D. K., and D. Pallamraju, (2017). Small-scale longitudinal variations in the daytime equatorial thermospheric wave dynamics as inferred from oxygen dayglow emissions. *J. Geophys. Res. Space Physics*, 122, 6528-6542, doi:10.1002/2017JA023891

Karan, D. K., Daniell, R. E., England, S. L., Martinis, C. R., Eastes, R. W., Burns, A. G., & McClintock, W. E. (2020). First zonal drift velocity measurement of equatorial plasma bubbles (EPBs) from a geostationary orbit using GOLD data. *J. Geophys. Res. Space Physics*, 125, e2020JA028173, doi:10.1029/2020JA028173

Karan, D. K., Eastes, R. W., Daniell, R. E., Martinis, C. R., Burns, A. G., & McClintock, W. E. (2021). Effects of 2020 September Moderate Geomagnetic Storms in the Nighttime Equatorial Ionization Anomaly (EIA) as Observed by GOLD Mission. AGU Fall Meeting 2021, New Orleans, LA, 13-17 December 2021, id. SA25D-1993, 2021AGUFMSA25D1993K.

Khadka, S. M., Valladares, C. E., Sheehan, R., & Gerrard, A. J. (2018). Effects of electric field and neutral wind on the asymmetry of equatorial ionization anomaly. *Radio Science*, 53, 683– 697, doi:10.1029/2017RS006428

Kil, H., DeMajistre, R., Paxton, L. J., & Zhang, Y. (2006). Nighttime F-region morphology in the low and middle latitudes seen from DMSP F15 and TIMED/GUVI. *Journal of atmospheric and solar-terrestrial physics*, *68*(14), 1672-1681, doi:10.1016/j.jastp.2006.05.024

Kil, H., E. R. Talaat, S.-J. Oh, L. J. Paxton, S. L. England, and S.-J. Su (2008). Wave structures of the plasma density and vertical E × B drift in low-latitude F region, *J. Geophys. Res. Space Physics*, 113, A09312, doi:10.1029/2008JA013106

545 Laundal, K. M., and Richmond, A. D. (2017). Magnetic Coordinate Systems, *Space Sci Rev*, 206,
546 27-59, doi:10.1007/s11214-016-0275-y

547 Liu, H., Lühr, H., Watanabe, S., Köhler, W., Henize, V., & Visser, P. (2006). Zonal winds in the
548 equatorial upper thermosphere: Decomposing the solar flux, geomagnetic activity, and seasonal
549 dependencies. *Journal of Geophysical Research: Space Physics*, *111*(A7).

550 Liu, H., Yamamoto, M. & Lühr, H. (2009). Wave-4 pattern of the equatorial mass density anomaly:
551 A thermospheric signature of tropical deep convection, *Geophysical Research Letters*, *36*, L18104,
552 doi:10.1029/2009GL039865

553 Luan, X., and S. C. Solomon (2008). Meridional winds derived from COSMIC radio occultation
554 measurements, *J. Geophys. Res. Space Physics*., 113, A08302, doi:10.1029/2008JA013089.

555 Lühr, H., M. Rother, K. Häusler, P. Alken, and S. Maus (2008). The influence of nonmigrating
556 tides on the longitudinal variation of the equatorial electrojet, *J. Geophys. Res. Space Physics*, 113,
557 A08313, doi:10.1029/2008JA013064

558 Lühr, H., & Manoj, C. (2013). The complete spectrum of the equatorial electrojet related to solar
559 tides: CHAMP observations. *Annales Geophysicae*, *31*, 1315–1331, doi:10.5194/angeo-31-1315-
560 2013

561 McClintock, W. E., Eastes, R. W., Beland, S., Bryant, K. B., Burns, A. G., Correira, J., et al.
562 (2020a). Global-scale observations of the limb and disk mission implementation: 2. Observations,
563 data pipeline, and level 1 data products. *J. Geophys. Res. Space Physics*, 125, e2020JA027809,
564 doi:10.1029/2020JA027809

565 McClintock, W. E., Eastes, R. W., Hoskins, A. C., Siegmund, O. H. W., McPhate, J. B., Krywonos,
566 A., et al. (2020b). Global-scale observations of the limb and disk Mission implementation: 1.
567 Instrument design and early flight performance. *J. Geophys. Res. Space Physics*, 125,
568 e2020JA027797, doi:10.1029/2020JA027797

569 Mo, X. H., & Zhang, D. H. (2020). Six-day periodic variation in equatorial ionization anomaly
570 region. *J. Geophys. Res. Space Physics*, 125, e2020JA028225. doi:10.1029/2020JA028225

571 Oberheide, J., J. M. Forbes, X. Zhang, and S. L. Bruinsma (2011). Wave-driven variability in the
572 ionospherethermosphere-mesosphere system from TIMED observations: What contributes to the
573 "wave 4"?, J. Geophys. Res., 116, A01306, doi:10.1029/2010JA015911.

574 Oyedokun, O. J., Akala, A. O., & Oyeyemi, E. O. (2020). Characterization of African equatorial
575 ionization anomaly during the maximum phase of Solar Cycle 24. Journal of Geophysical
576 Research: Space Physics, 125, e2019JA027066. doi:10.1029/2019JA027066

577 Pedatella, N. M., J. M. Forbes, A. Maute, A. D. Richmond, T.-W. Fang, K. M. Larson, and G.
578 Millward (2011), Longitudinal variations in the F region ionosphere and the topside ionosphere-

plasmasphere: Observations and model simulations, *J. Geophys. Res. Space Physics*., 116, A12309, doi:10.1029/2011JA016600

Pedatella, N. M., Hagan, M. E., & Maute, A. (2012). The comparative importance of DE3, SE2, and SPW4 on the generation of wavenumber-4 longitude structures in the low-latitude ionosphere during September equinox. *Geophysical Research Letters*, *39*, L19108, doi:10.1029/2012GL053643

Rodríguez-Zuluaga, J., Stolle, C., Yamazaki, Y., Xiong, C., & England, S. L. (2021). A synoptic-scale wavelike structure in the nighttime equatorial ionization anomaly. Earth and Space Science, 8, e2020EA001529, doi:10.1029/2020EA001529

Thébault, E., Finlay, C.C., Beggan, C.D., Alken, P., Aubert, J., Barroi, O. *et al.* (2015). International Geomagnetic Reference Field: the 12th generation, *Earth Planet Sp* **67,** 79, doi:10.1186/s40623-015-0228-9

Tsunoda, R. T. (1985). Control of the seasonal and longitudinal occurrence of equatorial scintillations by the longitudinal gradient in integrated E region Pedersen conductivity. *Journal of Geophysical Research: Space Physics*, *90*(A1), 447-456. doi:10.1029/JA090iA01p00447

Tsunoda, R. T., Saito, S., and Nguyen, T. T. (2018). Post-sunset rise of equatorial F layer—or upwelling growth? *Progress in Earth and Planetary Science, 5*(1), 1-28. doi:10.1186/s40645-018-0179-4

Venkatesh, K., P. R. Fagundes, D. S. V. V. D.Prasad, C. M..Denardini, A. J.deAbreu, R. de Jesus, and M. Gende (2015). Day-to-day variability of equatorial electrojet and its role on the day-to-day characteristics of the equatorial ionization anomaly over the Indian and Brazilian sectors, *J. Geophys. Res. Space Physics*, 120,9117–9131, doi:10.1002/2015JA021307

Yamazaki, Y. and Maute, A. (2016). Sq and EEJ—A Review on the Daily Variation of the Geomagnetic Field Caused by Ionospheric Dynamo Currents. *Space Sci Rev* **206,** 299–405, doi:10.1007/s11214-016-0282-z

Zhou, Yun-Liang & Lühr, Hermann & Alken, Patrick & Xiong, Chao. (2016). New perspectives on equatorial electrojet tidal characteristics derived from the Swarm constellation: Tidal features on equatorial electrojet. *J. Geophys. Res. Space Physics,* 10.1002/2016JA022713